engineering proceedings

MDPI

Proceeding Paper

Improving Magnetic Flux Density Fingerprint Map Matching by Mitigating AC-Induced Variability †

Peter J. Thompson [1,*], Paul D. Groves [1], Owen J. Griffiths [2], Robin J. Handley [2] and David R. Selviah [3]

[1] Department of Civil, Environmental & Geomatic Engineering, Faculty of Engineering Science, UCL (University College London), Gower Street, London WC1E 6BT, UK
[2] Dstl (Defence Science and Technology Laboratory), Porton Down, Salisbury SP4 0JQ, UK
[3] Department of Electronic & Electrical Engineering, Faculty of Engineering Science, UCL (University College London), Gower Street, London WC1E 6BT, UK
* Correspondence: peter.thompson.20@ucl.ac.uk
† Presented at the European Navigation Conference 2024, Noordwijk, The Netherlands, 22–24 May 2024.

Abstract: Magnetic flux density (MFD) map matching is a technique that can provide absolute position solutions by comparing a series of MFD measurements with a database. Map matching relies on the consistent measurement of the same physical phenomena during the surveying and positioning phases. However, fluctuations in MFD due to alternating current (AC) electricity, influenced by dynamic power requirements, pose a challenge. This paper analyses the characteristics of the influences of AC sources on MFD measurements. It shows that employing spectral filtering can isolate magnetic perturbations from AC sources, which could be used to enhance the magnetic map matching's resilience to this form of temporal change.

Keywords: magnetic; flux; density; map; matching; positioning; alternating; current; filtering; magnetometer

1. Introduction

Magnetic flux density (MFD) map matching is a technique that can provide absolute position solutions by comparing a series of MFD measurements with a geo-referenced database [1–5]. Consistent measurement of the same physical phenomena during the survey and the position phases of MFD map matching is fundamentally essential. However, fluctuations in MFD due to alternating current (AC) electricity, influenced by dynamic power requirements, pose a challenge, as these variations in AC supply lead to temporal changes in the MFD that are not captured in a single survey.

The characteristics of the influences of AC sources on MFD measurements are analysed by creating an environment physically replicating the underfloor cabling of a United Kingdom (UK) residential household, where the cables are in a void, which is placed on joists running perpendicular to the cables. Five variables are analysed: magnetometer type, electrical power transmitted through the cable, cable type, and distance from and distance along the cable. From this knowledge, spectral filtering is employed to isolate MFD from AC sources. This technique could enhance the MFD base map's resilience to temporal changes for map matching.

check for updates

Academic Editor: Terry Moore

Published: 20 May 2025

Citation: Thompson, P.J.; Groves, P.D.; Griffiths, O.J.; Handley, R.J.; Selviah, D.R. Improving Magnetic Flux Density Fingerprint Map Matching by Mitigating AC-Induced Variability. *Eng. Proc.* **2025**, *88*, 59. https://doi.org/10.3390/engproc2025088059

2. Background

2.1. Magnetic Map Matching

Map matching techniques, also known as fingerprinting, provide absolute position solutions by using variations in the strengths of a measurable parameter with associated locations [5]. In general, positioning by map matching involves two phases: surveying and positioning. During the surveying phase, the strengths of observations, or other measurable parameters, at known locations are recorded and stored in a spatial database. During the positioning phase, the user's equipment at an unknown location measures the strengths of the received signals or other measurable parameters, comparing these with the pre-recorded database to estimate the user's position [5].

The measurable parameters could include measured MFD, which refers to the magnetic **B** field. Still, other measurable parameters include (but are not limited to) radio signal strength, e.g., Wi-Fi or Bluetooth, and terrain height. One of the main influences on positioning performance by map matching is the type of measurable parameters stored in the database and how these vary spatially and temporally within the environment. The desired characteristic is that measurements vary spatially yet remain temporally consistent between the surveying and positioning phases. Furthermore, the dimensionality of the measurable parameters influences the performance of map-matching techniques [5].

As MFD (**B**) is an unstructured signal of opportunity, i.e., lacking a predefined format not designed for positioning, it lacks discernability compared to some of the previously mentioned measurable parameters. This means measurements are similar at multiple locations within the map-matching database. Therefore, a sliding window (or transect) of measurements from multiple locations is required to obtain a unique match within the database search area. The search area is defined by the current uncertainty in the user's position solution, centred on the current estimate of the user's position.

Three-axis magnetometers measure **B** along three orthogonal components in the body reference frame (${B_x}^b$, ${B_y}^b$, and ${B_z}^b$). Alongside these three axes, horizontal (${B_h}^b$), vertical (${B_v}^b$), and magnitude (${B_m}^b$) exist, depending on what attitude information is available. There is also a choice between matching the MFD directly or matching its spatial variation; the latter approach helps to minimise the impact of sensor biases.

The spatial variation of a measurable parameter is a crucial determinant of map-matching performance. The distance the measurable parameter is correlated over determines the achievable positioning resolution. Thus, the shorter the correlation length, the higher the potential position accuracy. This can vary between environments; for example, the complexity of indoor environments tends to shorten the correlation lengths for multiple types of measurable parameters. The temporal stability of a measurable parameter is a crucial characteristic of the performance of map-matching positioning [6]. This is a challenge for MFD map matching, as many sources are time-varying, particularly those due to electrical equipment or machinery.

2.2. Magnetic Sources

Changes in MFD are broadly split into two categories: variations and perturbations. Variations are due to the Earth's magnetic field, causing large-scale changes, which change slowly over time; these are modelled by the International Geomagnetic Reference Field (IGRF) [7]. Perturbations are local anomalies that cause local-scale changes. They vary significantly in intensity, direction, and duration within a localised area. The intensity and direction of a perturbation are determined by its size and distance from the source.

2.2.1. Earth's Magnetic Field

The magnetic field that extends from the Earth's interior into space is referred to as the Earth's geomagnetic field, which can be generalised as a large dipole magnet [8]. The Earth's magnetic field has variations that occur gradually across the entire globe, where a global model is available, with multiple generations because the Earth's magnetic field constantly, yet slowly, changes [9]. At the Earth's surface, for a magnetic anomaly-free environment, the magnetic field intensity varies between 25 μT and 65 μT [9,10].

2.2.2. Anthropogenic Sources of Magnetic Fields

Man-made objects can cause magnetic perturbations. For example, buildings and other structures use ferrous materials like steel and rebar. Though there are exceptions, such as lifts, ferrous materials within buildings tend to be static items. These static items, which cause deviations in the existing magnetic field, may significantly affect the vector components. For indoor environments, when no substantial infrastructural changes are conducted, several studies demonstrate that MFD measurements are either stable over time or vary slowly [3,6,11–16]. These static sources of magnetic perturbations are ideal for map matching, as there is significant spatial variation in observations, yet temporal stability still occurs.

Apart from structural elements, objects within a building can also create magnetic perturbations. This includes ferrous materials, like radiators, tables, and chairs. These objects might be moveable, creating concerns about temporal stability. Within an external suburban area, the creation of a model that includes the size, strength, and location of every source of magnetic perturbations is impractical [17]. Hence, MFD map matching requires a mapping phase instead of a modelling phase.

Electrical devices also create magnetic perturbations. Magnetic perturbations created by electrical cables can be considered the AC component of the observation, and non-electrical-caused magnetic perturbations can be regarded as the direct current (DC) component.

This paper uses the single-phase mains (UK: 230 V, 50 Hz) for the AC electrical source. Figure 1 shows an example of the influence of the UK's main single phase. This was conducted with a Samsung S8 Plus smartphone (Table 1). The sensor was placed directly on the unshielded kettle cable and has a sample rate of 15.4 Hz. This caused under-sampling, causing aliasing with a period of 0.1 s.

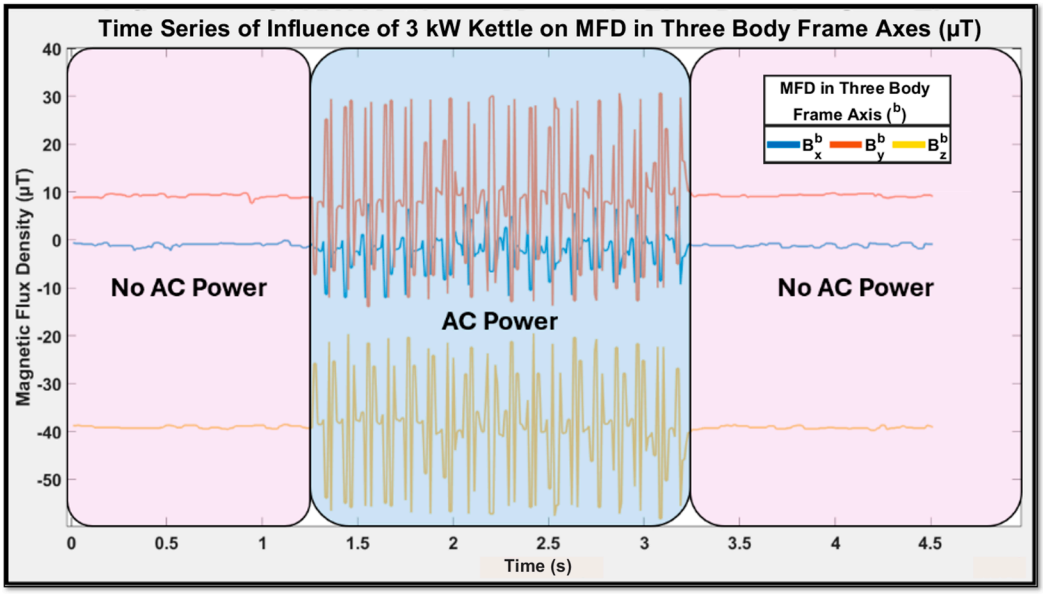

Figure 1. Time series of MFD in three body frame axes, with 3 kW AC power supply (S sensor).

Table 1. Specification of magnetometers.

Annotation	Device Manufacturer	Device Model	Magnetometer Model	Max Sample Rate (Hz)	Precision (nT)
S8	Samsung	S8 Plus (SM-G955F) [1]	Unknown	15.4	300
MG	Motorola	Moto G6	Unknown	8.7	300
M31a	Motorola	G31(w) [1]	QST QMC6308 (V1)	8.0	200
M31b	Motorola	G31(w) [1]	QST QMC6308 (V1)	8.0	200
BA	Bartington	MAG 03MSES70 [2]	MAG 03MSES70	1600	0.240

[1] Smartphone; [2] IMMU.

3. Materials and Methods

The magnetometers are placed at foot level, which is defined as on top of the floorboard (Figure 2b). This is to see the most significant impact of underfloor electrical cables. Sensor location on the foot is also a desirable location for an inertial and magnetic measurement unit (IMMU), as it enables a zero velocity update (ZVU) to be performed on every stride [18–20]. This study used five different magnetometers, the specifications of which are listed in Table 1.

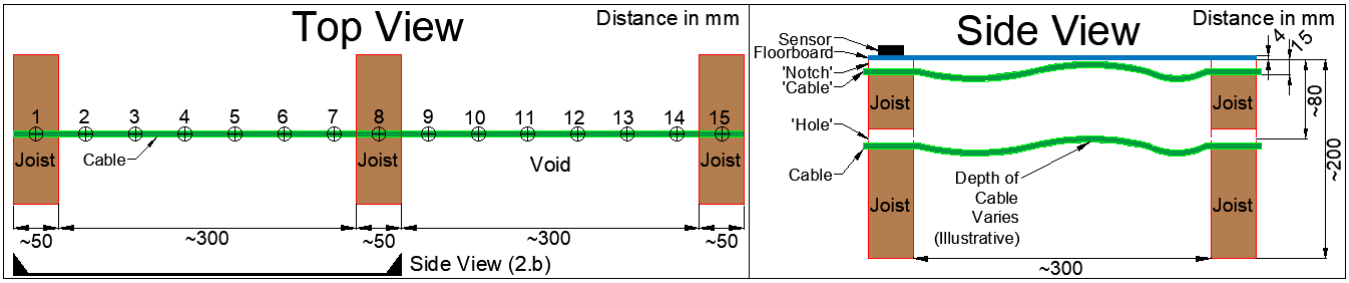

(**a**) (**b**)

Figure 2. Electric cable perpendicular to underfloor cable: (**a**) top view; (**b**) side view.

Electrical Sources in UK Residential Households

The location of the electrical cables in UK buildings is dictated by regulations, which are dependent on the type of building and date of wiring [21]. There are two scenarios for underfloor cables: perpendicular, which is the focus of this paper, and parallel.

In the parallel scenario, where the cable and joists are parallel, the cable depth relative to the joist will be approximately consistent at either half (80 mm) or full depth (200 mm). This depends on the wiring date, as regulations change over time. However, a cable route varies in the horizontal plane, so a straight line cannot be assumed.

In the perpendicular scenario, where the cable and joists are perpendicular, the distance between the magnetometer located on top of the floorboard directly above the cable and the cable itself is also not constant, as the cable laid in the joist is not a consistent depth below the floorboard. Two vertical positions, described in this paper as notch and hole, are used. For the notch scenario at the joist, cable depth can vary between 0 mm and 15 mm. Between the joists, this depth can increase to the full depth of the joist (250 mm). However, for this paper, the physical replica has a maximum depth of approximately 40 mm, which is more common [21] (Figure 2b).

While many of the experiments described in this paper were conducted outdoors, away from other AC perturbation sources, the tests with the Bartington magnetometer

(BA) (Bartington Instruments Ltd, Oxfordshire, UK) were conducted indoors for practical reasons. A second BA sensor was placed at the edge of the room (~5 m separation) to enable the background magnetic field to be calibrated. For the underfloor cable replica, multiple variables were analysed, and they are listed below:

1. **Magnetometer:** five sensors (Table 1);
2. **Power:** the electrical power transmitted through the cable (0–3000 W);
3. **Cable type:** unshielded cable, armoured cable, and unshielded cable S-looped;
4. **Radial distance from cable:** ten horizontal nodes, perpendicular to the cable, and two depth nodes, notch and hole (Figure 2b);
5. **Distance along cable:** 15 nodes on the floorboard above the cable at 250 mm intervals (Figure 2a).

4. Results

The reported MFD results depend on the magnetometer type, electrical power transmitted through the cable, cable type, and distance from and distance along the cable. This paper discusses how these variables affect B measurements.

4.1. Magnetometer Type

For this paper, a range of smartphone magnetometers were used (Table 1). The magnitude of the reported magnetic perturbation generated by the AC current varies between devices. For example, with the 3 kW kettle power supply, the mean range of $B_z{}^b$ between the peak and the trough of one cycle is 152 µT, 20 T, 6 µT, and 2 µT for the sensors S8, MG, M31a, and M31b, respectively. The undersampling causes aliasing, with a period of 34.9 s, 1.1 s, 0.47 s and 0.48 s for each sensor, respectively (Figure 3). The expected background is calculated from the IGRF model of the Earth's magnetic field, which is provided by the British Geological Survey (BGS) [7]. Each of these smartphone magnetometers undersamples the AC 50 Hz; therefore, the higher-specification BA magnetometer (Table 1) with a sample rate of 1600 Hz was also visualised in Section 4.2.

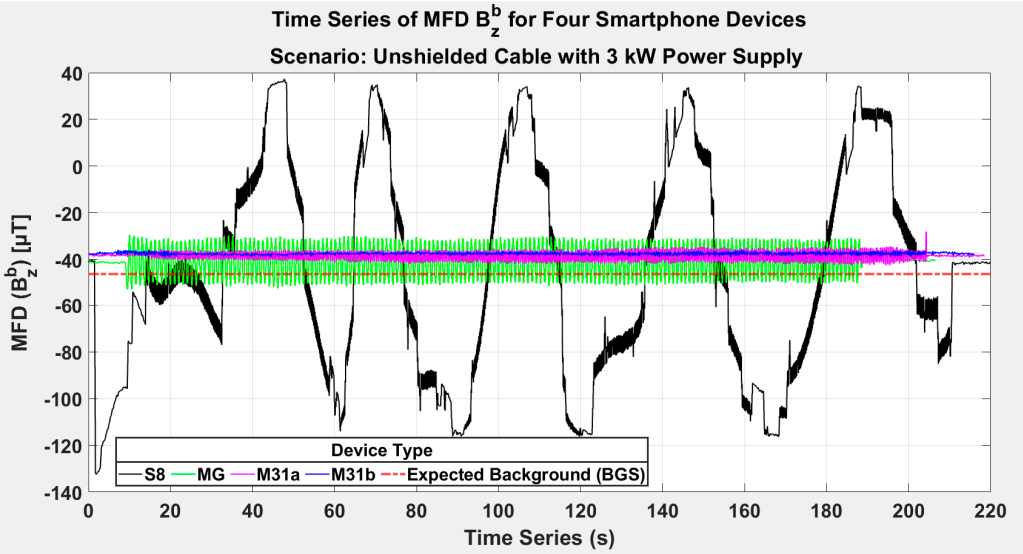

Figure 3. Time series of MFD ($B_z{}^b$) with an AC source of 3 kW and four different smartphones.

4.2. Power Variation

The mean range of $B_z{}^b$ between the peak and the trough of each AC cycle, per power, is presented in Table 2, which shows how increased power results in increased maximum magnetic perturbation. Note that the range at 0 W indicates the background AC in the

building, which the BA sensor detects. The MFDs of all three body frame axes ($B_x{}^b$, $B_y{}^b$, and $B_z{}^b$) at powers between 0 and 3000 W are shown in Figure 4. The larger the power supply to the cable, the larger the variations from the expected background.

Table 2. MFD ($B_z{}^b$) range between the peak and trough of AC cycle (BA sensor).

	Cable Type	Unshielded		Armoured		Unshielded (S-Looped)	
	Cable Location	Notch (15 mm)	Hole (80 mm)	Notch (15 mm)	Hole (80 mm)	Notch (15 mm)	Hole (80 mm)
Power (W)	0	0.002	0.002	0.001	0.001	0.004	0.004
	5	0.017	0.004	0.010	0.002	0.006	0.004
	24	0.083	0.011	0.021	0.002	0.010	0.001
	750	1.356	0.233	0.811	0.044	0.477	0.049
	1500	9.593	1.701	5.602	0.527	3.385	0.387
	3000	18.319	3.242	10.566	0.991	~	~

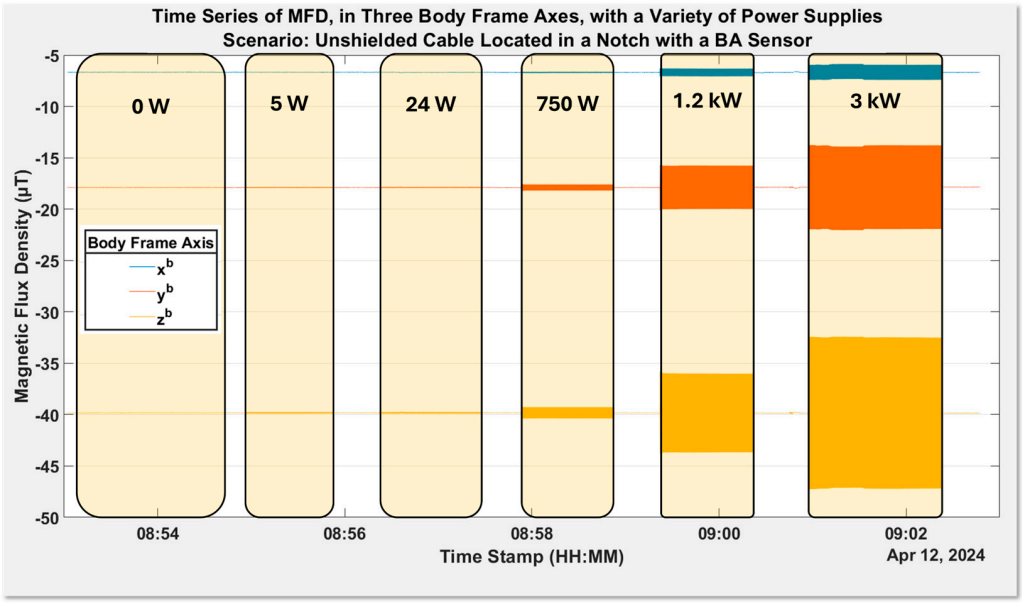

Figure 4. Time series MFD of three body frame axes with various power supplies (BA sensor).

4.3. Cable Type

The unshielded cable's material does not create a DC component of MFD detectable by any device. However, the armoured cable has a metal sheath with a DC component that is detectable by all devices. For $B_m{}^b$ with the BA sensor and the armoured cable in the notch location, a DC component of 2.6 μT is measured.

For the unshielded cable, once power is supplied to the cable, the AC component is detectable by all the devices (Figures 3 and 4). However, this AC component is only detectable for the armoured cable using the highest specification magnetometer (BA). The magnitude of this AC component of $B_z{}^b$ is less than the unshielded cable, with the peak change of the AC component at 3 kW of 18.3 μT for the unshielded cable and 10.6 μT for the armoured cable (Table 2).

In UK residential households, it is common for multiple cables to pass through a single notch/hole within a joist. These cables can have the power supply running in either direction [21]. To replicate this, the unshielded cable S-looped passes through the joists three times, with the power supply in the opposite direction for one of the cables. Due to inconsistent spatial variation between the three cables, the cable cannot be considered a single-line source in this scenario. The unshielded, S-looped cable has a smaller range of AC components in $B_z{}^b$ than that of the non-looped, unshielded cable. Furthermore, the S-looped cable is the only cable type where the range of the y component of MFD is

less than that of the z component. For example, at the 1.5 kW cable in the notch location, this range is 3.4 µT and 6.6 µT for ${B_z}^b$ and ${B_y}^b$, respectively. Table 2 presents data for the unshielded and armoured cables for various powers, where it is clear both cable type and power influence MFD.

4.4. Radial Distance from Cable

Radial distance, perpendicular to the cable at node 8, was split into vertical (Figure 2) and horizontal tests. MFD (${B_m}^b$) decreases as the radial distance from the source increases. Theoretically, for a point source, this should vary as the inverse cube of the distance, whereas for a line source, it should vary as the inverse square [22].

Table 2 presents the mean range of ${B_z}^b$ between the peak and the trough of each AC cycle for the BA sensor, for a range of powers and cable types, for the cable at both vertical depths, the notch at 15 mm, and the hole at 80 mm. For the unshielded cable, with a 3 kW power supply, the range of the AC component of ${B_z}^b$ is 18.3 µT for the notch (15 mm) and 3.2 µT for the hole (80 mm), with a building background of 2 nT. Table 2 indicates that with the sensor at the floorboard level, the cable location of the hole has a smaller influence on the MFD than it does on the notch due to AC sources. However, this decreased influence is still detectable by the BA sensor. This indicates that, for UK households, the date of wiring will influence the characteristics of the magnitude of magnetic perturbations from underfloor cables due to this date regulating the vertical location of the cable [21].

Ten nodes with 4.5 mm horizontal intervals perpendicular to the cable were used for the horizontal test. There is a standard 15 mm vertical offset due to the cable's location in the notch. Figure 5 shows the reduction of the unshielded cable's influence on the sensor by visualising the mean range of ${B_h}^b$ between the peak and the trough of each AC cycle for each horizontal position, with the unshielded cable and a 5 W power supply plotted against the radial distance. The building's background AC component has been removed.

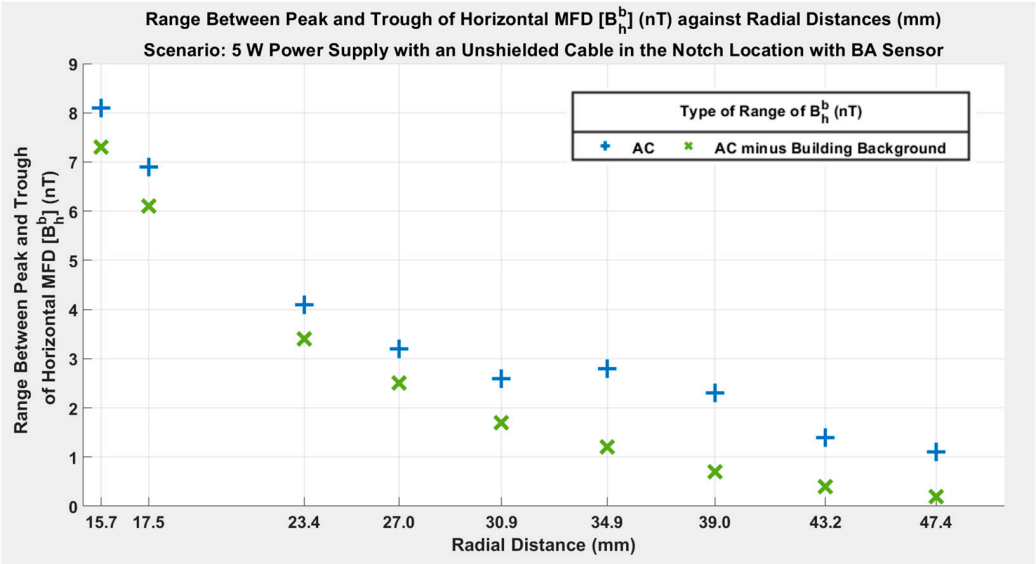

Figure 5. The MFD (${B_h}^b$) range with an unshielded cable and a 5 W power supply against radial distance (BA sensor).

4.5. Distance Along Cable

The depth of the cable below the floor varies (Figure 2). To understand how the slight variations in the distance between the floorboard and the cable affect the magnitude of the magnetic perturbations from the AC source, the MFD is measured at 15 50 mm intervals by sliding the magnetometer along the floorboard in the direction of the cable. The difference

between the background MFD (−46.294 μT) and the mean $B_z{}^b$ of the occupation period for three rounds is presented (Table 3). Within this scenario, the cable was closer to the floorboard between the 400–700 mm horizontal intervals. For the 3 kW power supplies, the influence of the cable on the MFD varies between each node. These results show that small spatial irregularities of a few centimetres from a straight line, typical of cable installations, impact the MFD, which is detectable by the S sensor. Thus, cables cannot be modelled as straight lines in the magnetic perturbation database. Furthermore, as dynamic power inputs are present in cables and power influences MFD, removing the AC component is desirable to increase the temporal resilience of the base map. The DC component should remain for spatial variation.

Table 3. The difference from the expected MFD ($B_z{}^b$) (μT) at 15 nodes along an unshielded cable in the notch position with the 3 kW power supply (S sensor).

Node No.		1	2	3	4	5	6	7	8	9	10	11	12	13	14	15
Dist. (mm)		0	50	100	150	200	250	300	350	400	450	500	550	600	650	700
Round	1	3.422	3.005	4.294	2.085	3.532	3.425	0.550	−5.879	−7.542	40.765	−41.587	9.551	9.067	15.547	22.470
	2	0.454	5.054	1.002	0.230	0.567	2.768	5.958	−4.798	−18.156	5.931	12.924	0.752	−1.048	1.403	7.715
	3	0.516	4.340	2.409	1.572	2.239	1.734	5.169	−5.926	−7.74	−13.491	−0.399	9.815	6.661	8.126	0.504
Range		2.968	2.049	3.292	1.855	2.965	1.691	5.408	1.128	10.614	54.256	54.511	9.063	10.115	14.144	21.966

4.6. Spectral Filtering

Spectral filtering aims to remove the temporally varying AC component whilst the constant DC component remains. To implement this, a low-pass Butterworth filter, with a sample rate of 1600 Hz, a frequency cutoff of 40 Hz, and a filter order of 12, was executed in MATLAB R2023a [23]. The test data are for a 3 kW power supply with the unshielded cable in the notch location using the BA sensor. This filter reduced the peak-to-trough amplitude of the AC component of the MFD from 1.3 μT to 0.1 μT, 10.5 μT to 0.8 μT, and 18.3 μT to 1.4 μT in the x, y, and z directions, respectively. This specific filter reduced the AC component by over a factor of ten for all body frame axes.

5. Conclusions

AC sources can influence MFD. The magnitude of the magnetic perturbations depends on various variables, including magnetometer type, electrical power transmitted through the cable, cable type, and distance from and along the cable. Spectral filtering can reduce the AC component, while the DC component remains. This isolates the temporal variation due to AC sources.

The IMMUs of commercial-off-the-shelf (COTS) microelectromechanical systems (MEMS) are constantly developing. If smartphone magnetometer sample rates increase to 100 Hz, this will enable the application of filtering techniques as per the Nyquist–Shannon sampling theorem for single-phase UK mains AC. Thus, filtering out AC components of magnetic perturbations may be achievable in the future with the IMMUs of COTS MEMS. However, the filtering demonstrated in Section 4.6 currently requires magnetometers with sample rates higher than those of the IMMUs of smartphone COTS MEMS used in this paper.

Future Work

Additional low-pass filter designs could be explored to optimise the trade-off between AC component filtering and bandwidth for measuring the spatial variation of the DC component as the sensor moves.

Future work could analyse other sources of AC, including but not limited to the UK mains triple phase (415 V, 50 Hz) and the United States and Canada (120 V, 60 Hz). This paper does not explore these; however, similar filtering techniques may be possible.

As mentioned previously, buildings cause magnetic perturbations, including from AC sources, which was discussed in this paper. In parallel to this work, the author is analysing how the characteristics of magnetic perturbations vary between different types of buildings.

Author Contributions: Conceptualization, P.J.T., P.D.G., O.J.G., R.J.H., and D.R.S.; methodology, P.J.T. and O.J.G.; software, P.J.T. and O.J.G.; validation, P.J.T., P.D.G., O.J.G., R.J.H., and D.R.S.; formal analysis, P.J.T.; investigation, P.J.T., P.D.G., O.J.G., R.J.H., and D.R.S.; resources, P.J.T., P.D.G., and O.J.G.; data curation, P.J.T. and O.J.G.; writing—original draft preparation, P.J.T.; writing—review and editing, P.J.T., P.D.G., O.J.G., R.J.H., and D.R.S.; supervision, P.D.G., O.J.G., R.J.H., and D.R.S.; project administration, P.D.G. and R.J.H.; funding acquisition, P.D.G. and R.J.H. All authors have read and agreed to the published version of the manuscript.

Funding: This research was funded by the Engineering and Physical Sciences Research Council (EPSRC) and Dstl as part of the ICASE scheme.

Institutional Review Board Statement: Not applicable.

Informed Consent Statement: Not applicable.

Data Availability Statement: The data are available on request from the corresponding author.

Conflicts of Interest: The authors declare no conflicts of interest.

References

1. Akai, N.; Ozaki, K. 3D magnetic field mapping in large-scale indoor environment using measurement robot and Gaussian processes. In Proceedings of the International Conference on Indoor Positioning and Indoor Navigation (IPIN), Sapporo, Japan, 18–21 September 2017. [CrossRef]
2. Ashraf, I.; Kang, M.; Hur, S.; Park, Y. MINLOC: Magnetic Field Patterns-Based Indoor Localization Using Convolutional Neural Networks. *IEEE Access* **2020**, *8*, 66213–66227. [CrossRef]
3. Ashraf, I.; Zikria, Y.B.; Hur, S.; Park, Y. A Comprehensive Analysis of Magnetic Field Based Indoor Positioning with Smartphones: Opportunities, Challenges and Practical Limitations. *IEEE Access* **2020**, *8*, 228548–228571. [CrossRef]
4. Hanley, D.; de Oliveira, A.S.D.; Zhang, X.; Kim, D.H.; Wei, Y.; Bretl, T. The Impact of Height on Indoor Positioning With Magnetic Fields. *IEEE Trans. Instrum. Meas.* **2021**, *70*, 1–19. [CrossRef]
5. Groves, P.D. *Principles of GNSS, Inertial, and Multisensor Integrated Navigation Systems*, 2nd ed.; GNSS Technology and Applications Series; Artech House: Boston, MA, USA; London, UK, 2013.
6. Angermann, M.; Frassl, M.; Doniec, M.; Julian, B.J.; Robertson, P. Characterization of the indoor magnetic field for applications in Localization and Mapping. In Proceedings of the International Conference on IPIN, Sydney, Australia, 13–15 November 2012. [CrossRef]
7. British Geological Survey. The IGRF Model (13th Generation). 2019. Available online: http://www.geomag.bgs.ac.uk/data_service/models_compass/igrf_calc.html (accessed on 29 June 2022).
8. Campbell, W.H. *Earth Magnetism: A Guided Tour Through Magnetic Fields*; Harcourt/Academic Press: San Diego, CA, USA, 2001.
9. Alken, P.; Thébault, E.; Beggan, C.D.; Amit, H.; Aubert, J.; Baerenzung, J.; Bondar, T.N.; Brown, W.J.; Califf, S.; Chambodut, A.; et al. International Geomagnetic Reference Field: The thirteenth generation. *Earth Planets Space* **2021**, *73*, 49. [CrossRef]
10. Arnaud, C.; Brown, W.; Alken, P.; Beggan, C.; Nair, M.; Cox, G.; Woods, A.; Macmillan, S.; Meyer, B.; Paniccia, M. *The US/UK World Magnetic Model for 2020–2025: Technical Report*; NOAA/National Oceanic and Atmospheric Administration: Washington, DC, USA, 2020. [CrossRef]
11. Li, B.; Gallagher, T.; Dempster, A.G.; Rizos, C. How feasible is the use of magnetic field alone for indoor positioning? In Proceedings of the International Conference on IPIN, Sydney, NSW, Australia, 13–15 November 2012. [CrossRef]
12. Afzal, M.H.; Renaudin, V.; Lachapelle, G. Assessment of indoor magnetic field anomalies using multiple magnetometers. In Proceedings of the 23rd International Technical Meeting of the Satellite Division of the Institute of Navigation (ION GNSS 2010), Portland, OR, USA, 21–24 September 2010; pp. 525–533, ISBN 9781617827358.
13. Gozick, B.; Subbu, K.P.; Dantu, R.; Maeshiro, T. Magnetic Maps for Indoor Navigation. *IEEE Trans. Instrum. Meas.* **2011**, *60*, 3883–3891. [CrossRef]
14. Ashraf, I.; Hur, S.; Park, Y. mPILOT-magnetic field strength based pedestrian indoor localization. *Sensors* **2018**, *18*, 2283. [CrossRef]
15. Subbu, K.P.; Gozick, B.; Dantu, R. LocateMe: Magnetic-Fields-Based Indoor Localization Using Smartphones. *ACM Trans. Intel. Syst. Technol.* **2013**, *4*, 1–27. [CrossRef]

16. Shu, Y.; Cheng, B.; Shen, G.; Zhao, C.; Li, L.; Zhao, F. Magicol: Indoor Localization Using Pervasive Magnetic Field and Opportunistic WiFi Sensing. *IEEE J. Sel. Areas Commun.* **2015**, *33*, 1443–1457. [CrossRef]
17. Storms, W.; Shockley, J.A.; Raquet, J.F. Magnetic field navigation in an indoor environment. In Proceedings of the 2010 Ubiquitous Positioning Indoor Navigation and Location Based Service (UPINLBS), Kirkkonummi, Finland, 14–15 October 2010; pp. 1–10. [CrossRef]
18. Reich, O.; Hubner, E.; Ghita, B.; Wagner, M.F.; Schafer, J. A Survey Investigating the Combination and Number of IMUs on the Human Body Used for Detecting Activities and Human Tracking. In Proceedings of the World Conference on Computing and Communication Technologies (WCCCT), Warsaw, Poland, 13–15 May 2020; pp. 20–27. [CrossRef]
19. Foxlin, E. Pedestrian Tracking with Shoe-Mounted Inertial Sensors. *IEEE Comput. Graph. Appl.* **2005**, *25*, 38–46. [CrossRef] [PubMed]
20. Wahlstrom, J.; Skog, I. Fifteen Years of Progress at Zero Velocity: A Review. *IEEE Sens. J.* **2021**, *21*, 1139–1151. [CrossRef]
21. IET (Institution of Engineering and Technology). Requirements for Electrical Installations: IET Wiring Regulations (18th Edition). 2022. Available online: https://electrical.theiet.org/bs-7671 (accessed on 7 April 2023).
22. Jackson, J.D. *Classical Electrodynamics*, 3rd ed.; Wiley: New York, NY, USA, 1999.
23. Mathworks. Butter—Butterworth Filter Design. Available online: https://uk.mathworks.com/help/signal/ref/butter.html (accessed on 2 May 2024).